

UniHash: Unifying Pointwise and Pairwise Hashing Paradigms for Seen and Unseen Category Retrieval

Xiaoxu Ma^{1,2}, Runhao Li³, Xiangbo Zhang², Zhenyu Weng^{1*}

¹South China University of Technology ²Georgia Institute of Technology ³Nanyang
Technological University

xma394@gatech.edu runhao001@e.ntu.edu.sg xiangbo.zhang@gatech.edu
wzytumbler@gmail.com

Abstract

Effective retrieval across both seen and unseen categories is crucial for modern image retrieval systems. Retrieval on seen categories ensures precise recognition of known classes, while retrieval on unseen categories promotes generalization to novel classes with limited supervision. However, most existing deep hashing methods are confined to a single training paradigm, either pointwise or pairwise, where the former excels on seen categories and the latter generalizes better to unseen ones. To overcome this limitation, we propose Unified Hashing (UniHash), a dual-branch framework that unifies the strengths of both paradigms to achieve balanced retrieval performance across seen and unseen categories. UniHash consists of two complementary branches: a center-based branch following the pointwise paradigm and a pairwise branch following the pairwise paradigm. A novel hash code learning method is introduced to enable bidirectional knowledge transfer between branches, improving hash code discriminability and generalization. It employs a mutual learning loss to align hash representations and introduces a Split-Merge Mixture of Hash Experts (SM-MoH) module to enhance cross-branch exchange of hash representations. Theoretical analysis substantiates the effectiveness of UniHash, and extensive experiments on CIFAR-10, MSCOCO, and ImageNet demonstrate that UniHash consistently achieves state-of-the-art performance in both seen and unseen image retrieval scenarios.

1. Introduction

Hashing has become a prominent solution for large-scale image retrieval due to its efficiency in both computation and storage [1–6]. It maps high-dimensional visual features into compact binary codes while preserving semantic sim-

ilarity in the Hamming space [7–10]. Recent deep hashing methods have achieved state-of-the-art performance by jointly optimizing feature extraction and hash code learning in an end-to-end fashion [11–20]. Despite these advances, real-world retrieval systems often face queries from both seen categories encountered during training and unseen categories that emerge after deployment. Achieving balanced performance across these two settings is crucial for developing reliable retrieval systems, a challenge that existing hashing methods have largely overlooked.

Deep supervised hashing methods can generally be divided into two paradigms: pointwise and pairwise. As shown in Fig. 1(a), recent pointwise methods (e.g., center-based methods)[11–13] introduce fixed or learnable hash centers that explicitly represent category prototypes. These methods establish representative hash centers for each category and train the network to align the hash codes of individual samples with their corresponding centers. Such pointwise supervision effectively enforces intra-class compactness [21–24], yielding superior retrieval performance on seen categories. However, their strong reliance on predefined centers limits their generalization to unseen categories [25]. In contrast, as shown in Fig. 1(b), pairwise methods learn relative similarities among samples. Specifically, binary pairwise models [15–17] aim to pull similar pairs closer and push dissimilar pairs apart in the Hamming space. Triplet-based extensions [18, 26] introduce an anchor–positive–negative structure to capture relative ranking information, while listwise variants [27] further optimize global ranking metrics by jointly considering multiple items. This relational supervision flexibly preserves semantic consistency through feature similarity, thereby enhancing generalization to unseen categories.

As existing deep hashing methods are trained under a single supervision paradigm, either pointwise or pairwise, they struggle to achieve balanced image retrieval performance across seen and unseen categories [25]. To address this challenge, we propose Unified Hashing (Uni-

*Corresponding author.

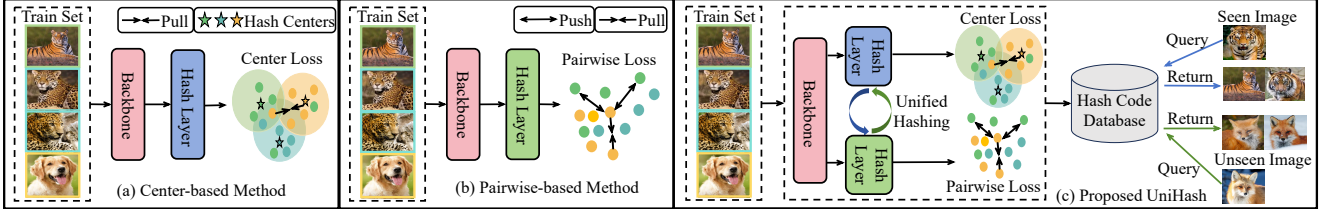


Figure 1. Comparison of existing deep hashing paradigms with the proposed Unified Hashing (UniHash). The figure depicts the evolution from traditional center-based and pairwise hashing to the proposed unified hashing paradigm, which fosters complementary supervision between branches and enhances retrieval performance on both seen and unseen image categories.

Hash), a dual-branch framework that unifies the strengths of both paradigms to achieve balanced image retrieval performance across seen and unseen categories. As illustrated in Fig. 1(c), UniHash consists of two complementary branches: a center-based branch corresponding to the pointwise paradigm and a pairwise branch corresponding to the pairwise paradigm. To enhance both the discriminability and generalization of hash codes, we introduce a novel hash code learning method that facilitates bidirectional knowledge exchange between two branches. Specifically, a mutual learning loss is employed to align hash code representations between two branches. Inspired by the Mixture of Experts (MoE) framework [28–31], a Split-Merge Mixture of Hash Experts (SM-MoH) module is designed to promote cross-branch interaction in hash representation learning. Through this design, the center-based branch acquires relational cues from the pairwise branch, while the pairwise branch benefits from the compact semantic structure maintained by the center-based branch. Furthermore, we theoretically show that UniHash alleviates paradigm-specific discrepancies by enforcing the consistency between the two learning branches.

In summary, our main contributions are as follows:

- We propose Unified Hashing (UniHash), a novel dual-branch framework that unifies the pointwise and pairwise training paradigms to integrate their complementary strengths.
- We introduce a hash code learning method that promotes cross-branch interaction and alignment of hash representations for more discriminative and generalizable hash codes.
- Theoretical analysis validates the effectiveness of UniHash, and extensive experiments demonstrate its state-of-the-art performance across both seen and unseen retrieval settings.

2. Related Works

Pointwise/Pairwise Training Paradigms. From the perspective of training paradigms, deep supervised hashing methods can be broadly categorized into pairwise and pointwise approaches. Early works such as Deep Hashing [32]

and HashNet [17] follow the pairwise paradigm, which learns hash functions by modeling pairwise or triplet relationships. In contrast, pointwise methods such as CSQ [11], OrthoHash [12], and MDSH [13] define category specific hash centers, either pre-defined or learnable, to cluster semantically similar samples around a common center while pushing apart dissimilar ones. Recent studies indicate that pointwise methods perform better on seen categories, whereas pairwise methods generalize more effectively to unseen categories [25]. In this work, we aim to unify the strengths of both paradigms to achieve balanced retrieval performance across seen and unseen categories.

Deep Mutual Learning (DML). DML [33] is initially introduced as a collaborative training strategy in which multiple networks learn jointly by aligning their predicted class probabilities to improve generalization. Building on this idea, subsequent work extended DML to visual object tracking [34], where lightweight networks mutually supervise each other during offline training to enhance feature representation and tracking accuracy. Unlike prior approaches [33–36] that train multiple networks under identical objectives, we enable two branches with distinct supervision paradigms to iteratively guide each other through hash code similarity for joint hash function optimization.

Mixture of Experts (MoE). The MoE framework [28] has recently been applied to large-scale neural networks, leveraging multiple specialized experts and a top-k gating mechanism for efficient computation. It has since been extended to multi-task learning in computer vision, such as AdaMV-MoE [29], which introduces task-specific routing and adaptive expert selection for diverse recognition tasks. Inspired by the effectiveness of MoE in modeling task-dependent information [28–31], we propose the Split-Merge Mixture of Hash Experts (SM-MoH) module within our framework. Unlike standard MoE, SM-MoH adopts a split-merge routing mechanism: branch-specific gates independently select experts to capture distinct supervisory cues, while shared experts merge their outputs to ensure transformation consistency across branches. This design enhances cross-branch interaction in hash representation learning and improves the overall quality of hash codes.

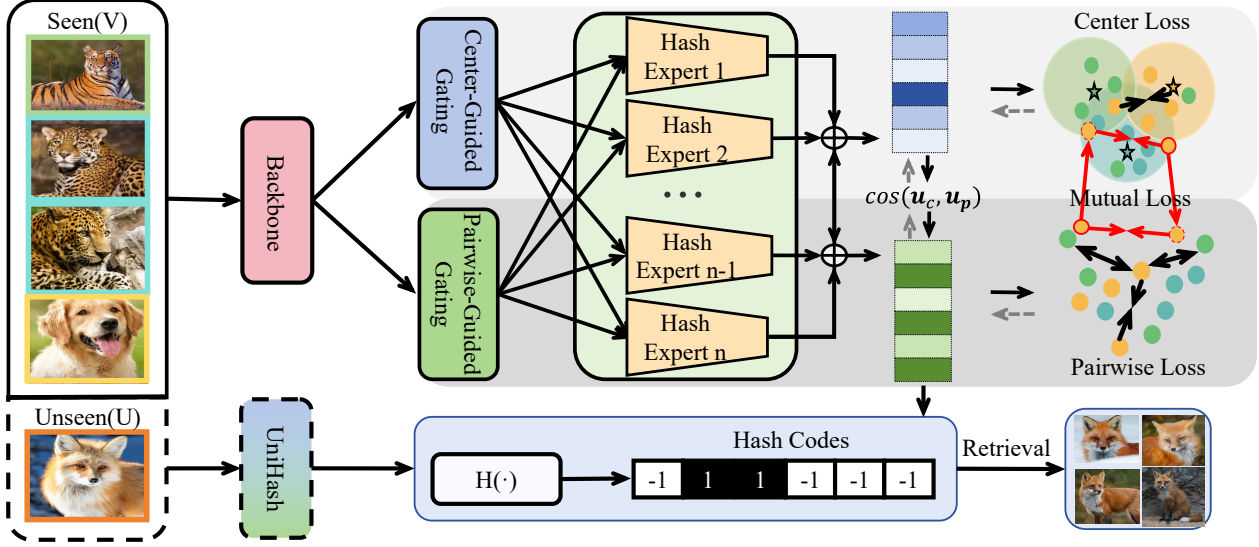


Figure 2. Overview of the proposed Unified Hashing (UniHash) framework. A deep neural network extracts image features, which are fed into two parallel branches producing center-based codes u_c and pairwise codes u_p . During training, the center-based branch learns relational cues from the pairwise branch, while the pairwise branch benefits from the semantic compactness of the center-based branch, leading to more discriminative and generalizable hash codes.

3. Methodology

We propose Unified Hashing (UniHash), a framework that unifies the complementary strengths of pairwise and center-based methods to achieve superior retrieval performance across both seen and unseen categories. We first present the overall framework in Sec. 3.1, and then provide a theoretical analysis of our methodology in Sec. 3.2.

3.1. UniHash Framework

Given an image dataset $\mathcal{X} = \{x_i\}_{i=1}^N$ with labels $\mathcal{Y} = \{y_i\}_{i=1}^N$, deep hashing learns a mapping

$$H : \mathcal{X} \rightarrow \{-1, 1\}^q,$$

encoding each image x_i into a q -bit code $b_i = \text{sign}(u_i)$. In our method, a backbone $\phi(\cdot)$ (ResNet-50 typically) extracts features $v_i = \phi(x_i)$, followed by two parallel branches that produce continuous hash codes $u_i^c, u_i^p \in (-1, 1)^q$ for the center-based and pairwise branches, respectively.

As illustrated in Fig. 2, UniHash comprises two main components: (1) a mutual learning loss that aligns hash representations between the two branches, and (2) a Split-Merge Mixture of Hash Experts (SM-MoH) module that enhances cross-branch interaction in hash representation learning. The details of these components are presented in the following subsections.

3.1.1. Mutual Learning Loss

In this paper, mutual learning loss refers to the composite objective combining the center-based loss L_C , the pairwise

loss L_P , and the cross-branch alignment term L_M :

$$L = \lambda_1 L_C + \lambda_2 L_P + \lambda_3 L_M, \quad (1)$$

where λ_1, λ_2 , and λ_3 are the hyperparameters.

Center-based Supervision. Each semantic class $c \in \{1, \dots, C\}$ is associated with a learnable hash center $h_c \in \{-1, 1\}^q$. For a sample x_i , the cosine similarity between its code and each class center is

$$\cos(u_i^c, h_c) = \frac{(u_i^c)^\top h_c}{\|u_i^c\| \|h_c\|}. \quad (2)$$

The class probability is computed as

$$P_{i,c} = \frac{\exp(\sqrt{q} \cos(u_i^c, h_c))}{\sum_{m=1}^C \exp(\sqrt{q} \cos(u_i^c, h_m))}. \quad (3)$$

The center loss encourages intra-class compactness and inter-class separability:

$$L_C = -\frac{1}{N} \sum_{i=1}^N \sum_{c=1}^C [y_{i,c} \log P_{i,c} + (1 - y_{i,c}) \log(1 - P_{i,c})]. \quad (4)$$

Pairwise Supervision. To preserve local similarity, we define a semantic similarity matrix

$$S_{ij} = \mathbb{I}(y_i^\top y_j > 0), \quad (5)$$

where $S_{ij} = 1$ if x_i and x_j share at least one label and 0 otherwise. Let $I_{ij} = \frac{1}{2}(u_i^p)^\top u_j^p$ denote the inner-product similarity of hash codes. The pairwise loss is given by

$$L_P = \frac{1}{N} \sum_{i,j} [\log(1 + e^{-|I_{ij}|}) + \max(0, I_{ij}) - S_{ij} I_{ij}]. \quad (6)$$

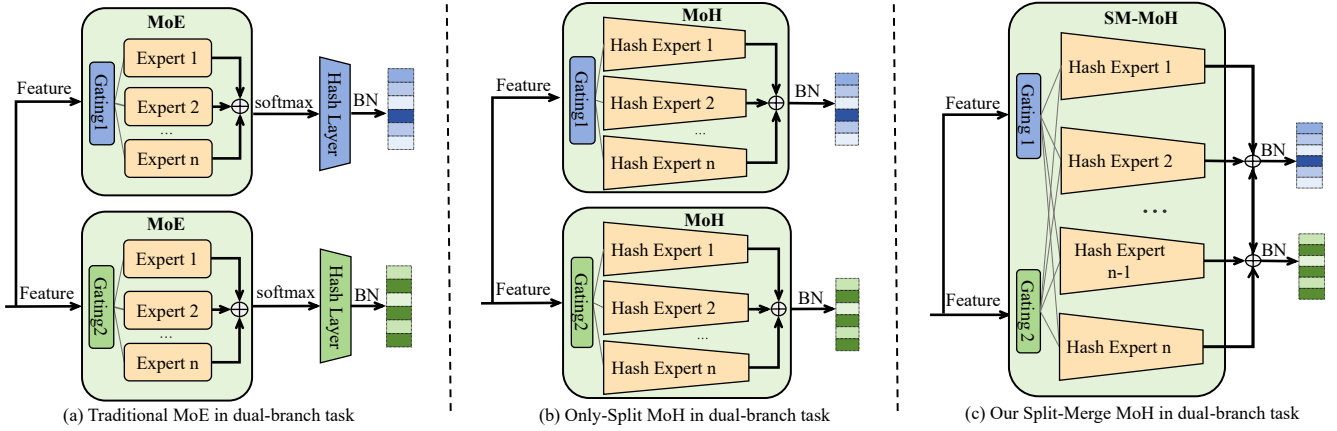


Figure 3. Comparison of expert-based hashing architectures. (a) Conventional MoE with separate experts per branch. (b) Only-Split MoH with independent gates and experts generating continuous hash codes. (c) Our proposed MoH with independent gates and shared experts.

This objective captures fine-grained neighborhood relations and enhances generalization to unseen categories.

Cross-branch Mutual Learning. To exchange information between branches, we introduce a cosine-based mutual loss:

$$L_M = \mathbb{E}[1 - \cos(u^c, u^p)], \quad (7)$$

where one branch is detached alternately per epoch to enable bidirectional knowledge flow.

Default Weights. Unless otherwise specified, we set $\lambda_1=4$, $\lambda_2=1$, $\lambda_3=1$. Impact of hyperparameter tuning is analyzed in Sec. 4.3.

3.1.2. SM-MoH Module

SM-MoH is a hashing-oriented adaptation of the classic MoE architecture, designed to split learning into branch-specific expert activations and merge them through a shared expert pool for coordinated semantic alignment.

Split Gating and Merged Experts. Two independent gating networks, center-guided gating G_c and pairwise-guided gating $G_p : \mathbb{R}^d \rightarrow \Delta^{m-1}$, produce expert weights for shared features v_n . To encourage sparse and specialized routing, we select the top- k experts with the highest activation scores:

$$K_s(v_n) = \text{TopK}(G_s(v_n), k), \quad (8)$$

where $s \in \{c, p\}$.

The selected scores are then normalized to form a sparse routing distribution $\tilde{G}_s(v_n)$, ensuring weights of chosen experts sum to one. A set of shared experts $\{E_i\}_{i=1}^m$, each implemented as a lightweight neural network, then projects the input directly into the continuous hash code space \mathbb{R}^q :

$$E_i : \mathbb{R}^d \rightarrow \mathbb{R}^q. \quad (9)$$

For each branch $s \in \{c, p\}$, the aggregated representation is obtained by merging the expert responses under its

gating distribution:

$$u_n^s = \sum_{i \in \mathcal{K}_s(v_n)} \tilde{G}_s(v_n)_i \cdot E_i(v_n), \quad (10)$$

Design Comparison. Unlike conventional MoE architectures that separate feature transformation and task-specific heads in Fig. 3(a), SM-MoH integrates expert transformation directly into the hashing process, as illustrated in Fig. 3(b)–(c). Each expert thus acts as an independent hashing pathway, producing semantically meaningful codes that reflect both branch-specific and shared characteristics. The final binary hash codes are computed as:

$$b_n^s = \text{sign}(u_n^s). \quad (11)$$

This split–merge mechanism serves as an implicit bridge for semantic alignment, enhancing the discriminability of the resulting hash codes.

3.2. Discrepancy Elimination Theory

This section explains why UniHash yields stronger performance. Any single branch hashing paradigm, center-based or pairwise, suffers from a paradigm-specific structure discrepancy: an error floor that cannot be removed by increasing the sample size n or the code length q . By transferring knowledge between the two branches, UniHash converts this fixed error into a vanishing consistency term, thereby asymptotically eliminating the structural discrepancy.

3.2.1. Preliminaries: Assumptions and Capacity Terms

We first establish the assumptions and fundamental capacity bounds that form the basis of our theoretical analysis.

Assumption 1 (Boundedness, Sparsity & Lipschitz). The feature extractor $\phi(x)$ is bounded: $\|\phi(x)\| \leq B_\phi$. Each expert E_i is ρ -Lipschitz and satisfies $\|E_i(z)\| \leq B_E$ for

Algorithm 1 UniHash

Require: Training set \mathcal{D} , number of experts m , top- k value k , hash length q , iterations T , weights $\lambda_1, \lambda_2, \lambda_3$

- 1: **Initialize:** DNN backbone $\phi(\cdot)$, shared experts $\{E_i\}_{i=1}^m$, gating networks G_c, G_p , hash centers $\{\mathbf{h}_i\}_{i=1}^c$
- 2: **for** $t = 1$ to T **do**
- 3: Sample mini-batch $X = \{x_1, \dots, x_N\}$ from \mathcal{D}
- 4: Extract features $V_0 = \{\mathbf{v}_1, \dots, \mathbf{v}_N\} \leftarrow \phi(X)$
- 5: **for** each stream $s \in \{c, p\}$ **do**
- 6: **for** each sample \mathbf{v}_n in V_0 **do**
- 7: Compute expert outputs: $\{E_i(\mathbf{v}_n)\}_{i=1}^m$
- 8: Select top- k experts: $\mathcal{K}_s(\mathbf{v}_n) \leftarrow \text{TopK}(G_s(\mathbf{v}_n), k)$
- 9: Normalize selected weights: $\tilde{G}_s(\mathbf{v}_n)_i \leftarrow \frac{G_s(\mathbf{v}_n)_i}{\sum_{j \in \mathcal{K}_s(\mathbf{v}_n)} G_s(\mathbf{v}_n)_j}$ for $i \in \mathcal{K}_s(\mathbf{v}_n)$
- 10: Compute refined hash: $\mathbf{u}_n^s \leftarrow \sum_{i \in \mathcal{K}_s(\mathbf{v}_n)} \tilde{G}_s(\mathbf{v}_n)_i \cdot E_i(\mathbf{v}_n)$
- 11: **end for**
- 12: **end for**
- 13: $L_C \leftarrow \text{CenterLoss}(\{\mathbf{u}_n^c\}, \{\mathbf{h}_i\})$
- 14: $L_P \leftarrow \text{PairwiseLoss}(\{\mathbf{u}_n^p\})$
- 15: **Compute mutual loss:**
- 16: **if** $t \bmod 2 = 0$ **then**
- 17: Detach \mathbf{u}_n^p as target
- 18: $L_M \leftarrow \frac{1}{N} \sum_{n=1}^N [1 - \cos(\mathbf{u}_n^c, \text{detach}(\mathbf{u}_n^p))]$
- 19: **else**
- 20: Detach \mathbf{u}_n^c as target
- 21: $L_M \leftarrow \frac{1}{N} \sum_{n=1}^N [1 - \cos(\text{detach}(\mathbf{u}_n^c), \mathbf{u}_n^p)]$
- 22: **end if**
- 23: Total loss: $L \leftarrow \lambda_1 L_C + \lambda_2 L_P + \lambda_3 L_M$
- 24: Update $\phi, \{E_i\}, G_c, G_p$ via RMSProp using L
- 25: **end for**
- 26: **return** Trained model: $\phi, \{E_i\}, G_c, G_p$

$\|z\| \leq B_\phi$. The gate activates at most k experts per input. Under sparse expert routing, the statistical complexity contributes

$$C_{\text{stat}} = O\left(\sqrt{\frac{k \log m}{n}}\right). \quad (12)$$

Assumption 2 (Center Separation). Pre-generated hash centers $\{\mathbf{h}_y \in \{-1, 1\}^q\}_{y=1}^c$ satisfy a minimum Hamming distance $\text{Ham}(\mathbf{h}_y, \mathbf{h}_{y'}) \geq d$ for $y \neq y'$.

Assumption 3 (Semantic Manifolds). The data reside on a union of semantic manifolds $\mathcal{M} = \bigcup_t \mathcal{M}_t$ with within-class diameter δ and inter-class separation $\Delta \gg \delta$ under a semantic metric. Under Assumption 2 and 3, quantization error decays exponentially in q :

$$C_{\text{quant}} = \exp(-\Omega(q)). \quad (13)$$

Assumption 4 (Mutual Consistency). Mutual learning en-

forces cross-branch agreement:

$$\mathbb{E}_x [\|\mathbf{u}^c(x) - \mathbf{u}^p(x)\|^2] \leq \tau^2.$$

which contracts the joint hypothesis space and induces a consistency penalty.

$$C_{\text{cons}} = O(\tau/\sqrt{n}). \quad (14)$$

3.2.2. UniHash Superiority Analysis

We investigate the superiority of UniHash by first characterizing the structural limitation of single-branch paradigms and then proving that UniHash removes this discrepancy through mutual consistency learning.

Proposition 1 (Irreducible Structural Discrepancy). *For a single-branch hashing method, the population risk obeys*

$$R_{\text{Base}} \leq \hat{R}_{\text{Base}} + C_{\text{stat}} + C_{\text{quant}} + E_{\text{struct}}, \quad (15)$$

where $E_{\text{struct}} > 0$ denotes a paradigm-specific, irreducible discrepancy independent of both n and q . Specifically, a center-based method, which lacks relational constraints, incurs a relative discrepancy $E_{\text{rel}} > 0$, whereas a pairwise method, lacking global semantic anchors, suffers from an absolute discrepancy $E_{\text{abs}} > 0$.

Theorem 1 (Discrepancy Elimination via UniHash). *Under all assumptions, the UniHash population risk satisfies*

$$R_{\text{UniHash}} \leq \hat{R}_{\text{UniHash}} + C_{\text{stat}} + C_{\text{cons}} + C_{\text{quant}}, \quad (16)$$

where C_{stat} , C_{cons} , and C_{quant} all vanish as $n, q \rightarrow \infty$.

Proof. By Proposition 1, any single-branch model has a paradigm-induced error floor $E_{\text{struct}} > 0$. The coupling loss L_M in UniHash enforces branch agreement, replacing this floor by a consistency term $C_{\text{cons}} = \mathcal{O}(\tau/\sqrt{n})$. Together with the statistical and quantization terms, the UniHash risk satisfies

$$R_{\text{UniHash}} \leq \hat{R}_{\text{UniHash}} + \mathcal{O}\left(\sqrt{\frac{k \log m}{n}}\right) + \mathcal{O}\left(\frac{\tau}{\sqrt{n}}\right) + \exp(-\Omega(q)). \quad (17)$$

Hence $C_{\text{stat}}, C_{\text{cons}} \rightarrow 0$ as $n \rightarrow \infty$ and $C_{\text{quant}} \rightarrow 0$ as $q \rightarrow \infty$, implying $R_{\text{UniHash}} - \hat{R}_{\text{UniHash}} \rightarrow 0$ and thus asymptotic elimination of the paradigm-specific discrepancy. \square

4. Experiments

Datasets. Following prior works [11–13, 15–20], we evaluate performance on CIFAR-10 [37], ImageNet [38], and MSCOCO [39] for category-level retrieval. Evaluation metrics include mean average precision (mAP) and precision-recall curves. We report mAP@1000 for CIFAR-10 and ImageNet, and mAP@5000 for MSCOCO.

Training Setup. Following [11–13], we use a pre-trained ResNet-50 [40] as the backbone network $\phi(\cdot)$ and append a 4096-dimensional fully-connected ReLU layer [41] after the 2048-dimensional pooled feature to generate the base features for hashing. These features are processed by a Split-Merge Mixture of Hash Experts (SM-MoH) module, consisting of m shared expert networks $\{E_i\}_{i=1}^m$, two gating networks G_c and G_p , and hash centers $\{\mathbf{h}_i\}_{i=1}^c$ for the center stream. Input images are resized to 224×224 , and we use a mini-batch size of $N = 64$. The model is trained for $T = 100$ epochs to optimize the backbone ϕ , experts $\{E_i\}$, and gating networks G_c, G_p , by jointly optimizing λ_1, λ_2 , and λ_3 . The final binary hash code is obtained as $\text{sign}(\mathbf{u}_n^s)$, where \mathbf{u}_n^s ($s \in \{c, p\}$) are the refined continuous hash codes from the center and pairwise streams. Our model is implemented in PyTorch and trained on an NVIDIA RTX 4090 GPU using the RMSProp optimizer with a learning rate of 0.0001.

4.1. Closed-Set Retrieval Performance

We compare our method with nine deep hashing algorithms: five pointwise methods (DPN [20], GreedyHash [19], CSQ [11], OrthoHash [12], MDSH [13]), three pairwise methods (DSH [15], DPSH [16], HashNet [17]), and one tripletwise method (DTSH [18]). Table 1 reports the Mean Average Precision (mAP) results for image retrieval. We adopt ResNet-50 as the backbone for all compared methods, including DSH, DPSH, DTSH, HashNet, GreedyHash, DPN, CSQ, OrthoHash, MDSH, and our proposed UniHash. Compared to these methods, our method achieves mAP improvements of 1.74%, 1.21%, and 0.87% on MSCOCO, CIFAR-10, and ImageNet, respectively, averaged across different code lengths.

We further evaluate retrieval performance using Precision-Recall (PR) curves, as shown in Fig. 4. Our method consistently yields a larger Area Under the PR Curve (AUC-PR) across all bit lengths, demonstrating superior precision across a wide range of recall values. These results underscore the robustness and generalization capability of our method for large-scale image retrieval.

4.2. Generalization to Unseen Categories

To evaluate retrieval generalization on unseen classes, following [25], we split datasets into seen and unseen categories, holding out 20% of CIFAR-10 and 15% of ImageNet and MSCOCO as unseen and excluding them from training. Table 2 reports mAP for four cases: (a) Seen@Seen and Seen@All: queries from seen classes searching among databases of seen-only or all images, and (b) Unseen@Unseen and Unseen@All: queries from novel classes searching among only unseen images or the entire database. It is worth noting that this constitutes a more challenging zero-shot hashing task [25]. Although zero-

shot hashing has been studied in prior works [17, 44], their experimental settings typically designate only a single category as unseen during testing, which provides a limited assessment of a method’s retrieval capability when facing multiple unseen categories.

As shown in Table 2, UniHash demonstrates robust performance on both seen and unseen retrieval tasks. For seen-category queries, UniHash achieves near-perfect accuracy (*e.g.*, 97% mAP on CIFAR-10) and sustains this on the Seen@All task. Competing methods also perform well but often drop slightly on Seen@All due to interference from unseen classes. More importantly, UniHash significantly outperforms prior methods on unseen-category queries. On CIFAR-10, UniHash achieves 84.7% mAP on Unseen@Unseen (vs. 82.0% for OrthoHash) and maintains a much higher mAP on Unseen@All (35.3% vs. 7.2% for CSQ). Similar trends hold on ImageNet and MSCOCO, where UniHash yields the highest Unseen@Unseen accuracy and clearly better Unseen@All mAP (with about 4% absolute gains over the best baselines). These results indicate that UniHash enables strong generalization, retrieving novel-class images even with many distractors.

4.3. Ablation Study

We conduct an ablation study on three datasets under different hash code lengths (16, 32, and 64 bits) to evaluate the effectiveness of the proposed components in our deep hashing network, including both the overall framework modules in Table 3 and the detailed design choices of the Split-Merge Mixture of Hash Experts (SM-MoH) head in Table 4.

Analysis of Overall Framework. To evaluate the contribution of each component in overall architecture, we conducted a closed-set ablation study on both the SM-MoH and Mutual Learning (ML) loss modules, as shown in Table 3. Baseline (without either SM-MoH or ML) shows that the center-based branch consistently outperforms the pairwise branch (*e.g.*, 0.8940 vs. 0.8873 on ImageNet at 64 bits), indicating stronger standalone effectiveness. ML alone improves the weaker pairwise branch (*e.g.*, 0.8894 vs. 0.8873 pairwise branch on ImageNet at 64 bits), by enabling bidirectional knowledge transfer. Gains for the center-based branch are smaller due to limited diversity without SM-MoH. SM-MoH alone slightly reduces performance (*e.g.*, center-based: 0.8325 vs. 0.8940), suggesting that without collaborative training, the structured interaction it introduces is underutilized. SM-MoH + ML achieves the best results (*e.g.*, 0.8997/0.9062 on ImageNet at 64 bits), as SM-MoH enhances inter-branch communication and mutual learning amplifies mutual supervision, improving both intra-class compactness and inter-class separability.

Design Variation in SM-MoH. We next evaluate several design alternatives for the SM-MoH in Table 4. The conventional setup (2DNNs+MoE) employs two separate

Table 1. Comparison results of closed-set retrieval performance w.r.t. mAP on three datasets across different bit configurations. **Bold** values indicate the best performance, and underlined values indicate the second best performance.

Method	CIFAR-10(@1000)			ImageNet(@1000)			MSCOCO(@5000)		
	16 bits	32 bits	64 bits	16 bits	32 bits	64 bits	16 bits	32 bits	64 bits
DSH[15]	0.7313	0.7402	0.7272	0.7179	0.7448	0.7585	0.7221	0.7573	0.7790
DPSH[16]	0.3098	0.3632	0.3638	0.6241	0.7626	0.7992	0.6239	0.6467	0.6322
HashNet[17]	0.8959	0.9115	0.8995	0.6024	0.7158	0.8071	0.7540	0.7331	0.7882
DTSH[18]	0.7783	0.7997	0.8312	0.6606	0.7803	0.8120	<u>0.7702</u>	0.8105	0.8233
GreedyHash[19]	0.3519	0.5350	0.6177	0.7394	0.7977	0.8243	0.7625	0.8033	0.8570
DPN[20]	0.7576	0.7901	0.8040	0.7987	0.8298	0.8394	0.7571	0.8227	0.8623
CSQ[11]	0.7861	0.7983	0.7989	0.8377	0.8750	0.8836	0.7509	<u>0.8471</u>	<u>0.8610</u>
OrthoHash[12]	0.9087	0.9297	0.9454	0.8540	0.8792	0.8936	0.7174	0.7675	0.8060
MDSH[13]	<u>0.9455</u>	<u>0.9554</u>	<u>0.9607</u>	<u>0.8639</u>	<u>0.8863</u>	<u>0.9019</u>	0.7542	0.8131	0.8143
CFBH[42]	0.7187	0.7397	0.7580	0.8120	0.8572	0.8950	0.6807	0.8325	0.8521
Ours	0.9665	0.9657	0.9658	0.8744	0.8975	0.9062	0.7903	0.8675	0.8727

Table 2. Retrieval under seen/unseen splits. mAP for Seen@Seen, Seen@All, Unseen@Unseen, and Unseen@All on 20%-unseen CIFAR-10 and 15%-unseen ImageNet/MSCOCO. **Bold**: best; Underlined: second best.

Method	CIFAR-10(@1000)			ImageNet(@1000)			MSCOCO(@5000)		
	16 bits	32 bits	64 bits	16 bits	32 bits	64 bits	16 bits	32 bits	64 bits
(a) Seen@Seen / Seen@All									
CSQ [11]	95.2/95.1	95.1/95.0	95.0/94.9	85.3/85.0	89.1/88.7	90.6/90.2	<u>65.0</u> /79.7	68.8/81.9	70.1/82.4
OrthoHash [12]	94.6/92.8	95.1/93.2	<u>95.7</u> /93.7	<u>88.2</u> /87.7	90.3/89.8	<u>91.5</u> /90.9	62.7/78.7	65.8/80.5	68.5/82.4
MDSH [13]	92.8/92.3	92.5/92.0	92.8/89.9	75.5/75.3	78.8/78.5	81.9/81.1	<u>64.2</u> /80.1	<u>70.3</u> /81.2	<u>70.9</u> /83.3
CHN [43]	<u>95.8</u> /95.7	<u>95.9</u> /95.5	95.6/90.1	86.4/86.0	88.9/88.5	90.1/89.5	—	—	—
DSH [15]	92.6/91.9	92.5/91.8	92.9/92.0	68.8/67.9	79.5/78.2	85.3/84.0	46.8/64.6	51.1/69.7	51.4/71.8
HashNet [17]	80.5/80.1	92.7/92.2	94.3/93.4	49.1/48.9	75.8/75.0	86.5/85.6	52.4/74.8	59.9/79.9	64.6/82.4
Ours	97.3/97.0	97.2/97.1	97.2/97.0	89.9/88.3	92.2/89.9	92.4/91.5	70.3/81.0	72.5/82.3	73.2/83.9
(b) Unseen@Unseen / Unseen@All									
CSQ [11]	77.3/7.2	73.1/10.2	75.7/9.4	38.1/19.6	<u>51.7</u> /36.2	55.8/42.2	46.9/50.1	51.2/54.0	52.9/55.8
OrthoHash [12]	<u>82.0</u> /31.6	<u>83.0</u> /36.0	82.1/36.3	41.3/25.1	50.7/34.8	59.9/40.5	<u>49.2</u> /54.7	50.9/55.9	53.3/58.1
MDSH [13]	76.3/18.8	79.4/35.0	81.4/45.2	28.3/10.0	31.8/14.8	41.1/21.1	<u>48.6</u> /55.9	50.5/56.2	53.4/57.4
CHN [43]	73.2/6.6	73.2/11.6	78.0/39.0	37.0/18.0	46.9/30.8	56.2/39.0	—	—	—
DSH [15]	74.5/11.0	70.8/18.3	72.4/20.0	42.6/20.9	49.6/26.8	56.1/34.6	41.1/45.0	44.1/47.1	46.3/50.2
HashNet [17]	78.8/9.4	77.7/24.7	80.8/38.2	42.3/18.9	<u>57.5</u> /32.3	<u>71.2</u> /44.8	44.5/45.9	<u>51.8</u> /55.8	<u>55.9</u> /59.2
Ours	84.7/35.3	85.2/36.6	85.6/49.8	44.7/28.0	59.1/38.0	71.3/48.2	53.2/58.7	57.9/60.3	58.4/62.1

Table 3. Ablation study of Mutual learning (ML) and SM-MoH across different datasets for 64 bits. The best results are **bolded**.

Modules	CIFAR-10(@1000)		ImageNet(@1000)	
Baseline	ML	SM-MoH	center-based	pairwise
✓			0.9607	0.9605
✓	✓		0.9586	0.9634
✓		✓	0.9357	0.9639
✓	✓	✓	0.9611	0.9658
			0.8997	0.9062

DNNs with expert modules. It achieves noticeable improvements over the baseline (e.g., 0.9643 vs. 0.9607

Table 4. Ablation study of SM-MoH design variants with 64-bit codes. $\sigma(\cdot)$ is softmax function. Best results are in **bold**.

Model	Experts	$\sigma(\cdot)$	CIFAR-10	ImageNet	MSCOCO
2DNNs+MoE	separate	✓	0.9634	0.8862	0.8605
1DNN+MoE	separate	✓	0.9643	0.9003	0.8693
1DNN+MoH	separate	✗	0.9651	0.9033	0.8697
1DNN+MoH	shared	✓	0.9647	0.9012	0.8684
1DNN+MoH	shared	✗	0.9658	0.9062	0.8727

on CIFAR-10), demonstrating the benefit of collaborative

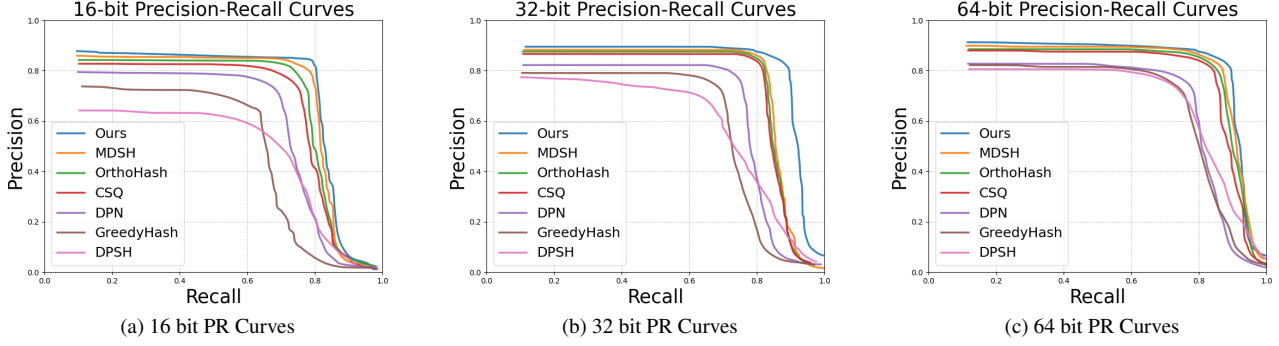


Figure 4. Precision-Recall curves on ImageNet across different bit configurations.

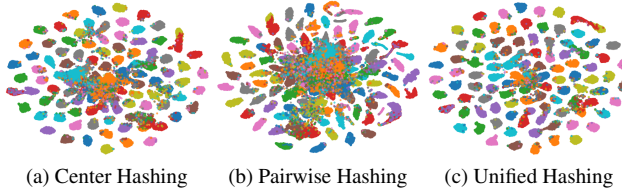


Figure 5. Impact of Unified Hashing (UniHash) on hash code distribution on ImageNet with 16-bit configuration.

learning. However, to further enhance performance and simplify the architecture, we explore alternative designs. Switching to a single-branch structure (1DNN+MoE) leads to slightly improved results (*e.g.*, 0.9634 vs. 0.9643 on CIFAR-10; 0.8605 vs. 0.8693 on MSCOCO), confirming that a unified backbone provides more coherent feature learning for hashing tasks. Replacing MoE with our proposed SM-MoH module—which maps features directly to the hash space—further improves performance (*e.g.*, 0.9651 on CIFAR-10, 0.9033 on ImageNet), demonstrating its better alignment with deep hashing objectives. This gain holds for both separate and shared expert configurations. Sharing experts across branches removes redundancy and enhances learning consistency, with shared MoH slightly outperforming its separate counterpart (*e.g.*, 0.9647 vs. 0.9651 on CIFAR-10; 0.8684 vs. 0.8697 on MSCOCO). Removing the softmax layer yields the best performance across all datasets (*e.g.*, 0.9658 on CIFAR-10, 0.9062 on ImageNet, 0.8727 on MSCOCO), likely due to improved code separability by avoiding over-smoothing among experts.

Hyperparameter Tuning. Figure 6 shows a hyperparameter study on ImageNet with 16-bit hash codes, varying one of λ_1 , λ_2 , or λ_3 while fixing the others. λ_1 and λ_2 control the center- and pairwise-based losses, and λ_3 regulates mutual loss. The results reveal a dominant–auxiliary dynamic: when $\lambda_1 \gg \lambda_2$, the center branch outperforms; conversely, when $\lambda_2 \gg \lambda_1$, the pairwise branch outperforms. Configurations with $\lambda_1 > \lambda_2$ achieve higher mAP, so the center branch serves as the primary while the pairwise branch fine-tunes it. Both λ_1 and λ_2 exhibit unimodal trends, with optimal values within $[1, 10]$. And λ_3 performs best at 1, beyond which excessive coupling degrades performance. The optimal setting is $\lambda_1 = 4$, $\lambda_2 = 1$, $\lambda_3 = 1$.

wise branch fine-tunes it. Both λ_1 and λ_2 exhibit unimodal trends, with optimal values within $[1, 10]$. And λ_3 performs best at 1, beyond which excessive coupling degrades performance. The optimal setting is $\lambda_1 = 4$, $\lambda_2 = 1$, $\lambda_3 = 1$.

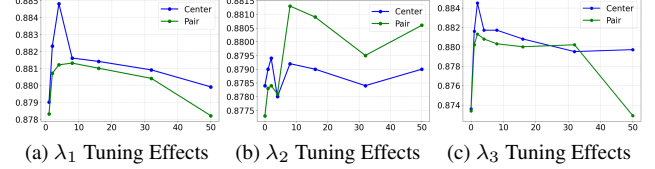


Figure 6. Impact of hyperparameter tuning on mAP for ImageNet with 16-bit configuration.

4.4. Hash Codes Visualization

To illustrate the effectiveness of UniHash, we visualize the t-SNE [45] of hash codes generated by three methods on ImageNet, as shown in Fig. 5: (a) center-based [13], (b) pairwise-based [46], and (c) our UniHash approach. The center-based method in (a) produces a circular distribution, indicating clearly decent global alignment but limited fine-grained separation. The pairwise-based method in (b) yields a more elongated structure with overlapping clusters, suggesting weaker overall structure. In contrast, UniHash in (c) consistently leads to a more well-clustered distribution, with fewer ambiguous points across class boundaries. These results show that UniHash improves intra-class compactness and inter-class separability by making the center- and pairwise-based branches complementary, yielding more discriminative hash codes.

5. Conclusions

We propose Unified Hashing (UniHash), a dual-branch framework designed to achieve good image retrieval performance across both seen and unseen categories. UniHash comprises two complementary branches: one following the pointwise training paradigm and the other following the pairwise paradigm. To strengthen cross-branch interaction

and representation alignment, we introduce a novel hash code learning method that facilitates deeper information exchange between branches, yielding more discriminative and generalizable hash codes. Theoretical analysis verifies the effectiveness of UniHash, and extensive experiments on CIFAR-10, MSCOCO, and ImageNet demonstrate state-of-the-art performance under both closed-set and seen/unseen retrieval protocols, confirming its robustness across diverse retrieval settings.

A. Summary

This appendix provides detailed insights and additional experimental results to support the main paper.

B. Training Setup

B.1. Datasets

ImageNet is a large-scale image classification dataset consisting of over 1.2 million images annotated with 1,000 categories. Following the protocol in [38], we use the ILSVRC2012 version for evaluation. The validation set of 50K images is used as the query set, while the remaining training images form the database. For training, we randomly sample 130K images from the database.

CIFAR-10 consists of 60,000 images across 10 categories, with each image sized 32×32 . Following the standard practice in [37], we use 10K test images as the query set and the remaining 50K training images as the database. For training, 5K images are randomly sampled from the database.

MSCOCO [39] is an image recognition, segmentation, and captioning dataset. We use the public version processed by [39], where images with missing category information have been filtered out. This results in 122K labeled images by combining the training and validation splits. We randomly sample 5K images as the query set, with the remaining images forming the database, and then randomly sample 10K images from the database for training.

Seen/Unseen Splitting [25] refers to our unified protocol for constructing seen and unseen subsets across both single-label and multi-label datasets. For single-label datasets such as CIFAR-10 and ImageNet-1K, we partition the label space using dataset-specific ratios: in CIFAR-10, 80% of the categories are designated as seen, whereas in ImageNet, 85% of the categories are treated as seen; the remaining categories in each dataset serve as unseen. For the multi-label dataset MSCOCO, we likewise divide the label space by a category ratio (85% seen). However, since images may contain multiple tags, an image is included in the seen or unseen subset only when all of its labels fall entirely within the corresponding class group, while images with mixed labels are used exclusively in the “all-class” database settings. Using these purified subsets, we then construct the four evaluation protocols—Seen@Seen, Seen@All, Unseen@Unseen, and Unseen@All—in a consistent manner across all datasets.

License. ImageNet is released under a non-commercial license, and the use of the dataset is restricted to research and educational purposes. Users must apply for access and agree to the ImageNet Terms of Use. CIFAR-10 is made publicly available by the University of Toronto under the

MIT License. This permits free use, modification, and distribution of the dataset for both research and commercial purposes. For MSCOCO, the annotations are provided under the Creative Commons Attribution 4.0 License (CC BY 4.0), and the use of the images must comply with the Flickr Terms of Use. The dataset is released for academic and research use.

C. Ablation Study and Further Analysis

C.1. Comparison with Traditional Mutual Learning

Traditional Deep Mutual Learning (DML) [33, 34, 36, 47] typically employs two separate branches, where each branch contains an independently initialized and trained deep neural network (DNN). While this design allows for mutual supervision between diverse learners, it also limits the potential for fine-grained interaction between the learned representations, especially in the context of hashing where compact and consistent binary codes are desired.

In contrast, our method adopts a shared-backbone design with two branches operating on the same DNN. This encourages closer interaction and more effective information sharing between the branches, thereby facilitating the generation of more consistent and semantically aligned hash codes. The underlying idea is to enforce mutual guidance without introducing significant representational discrepancies caused by separate networks.

We evaluate both settings — one with a single shared DNN (denoted as 1DNN+MoH), and one with two independent DNNs (denoted as 2DNN+MoH) — across three benchmark datasets: ImageNet, MSCOCO, and CIFAR-10. As shown in Table 5, our shared DNN design consistently outperforms the traditional dual-DNN setup across almost all bit lengths and datasets.

C.2. SM-MoH Module Analysis

To better understand the efficacy of our proposed Split-Merge Mixture of Hash Experts (SM-MoH) module, we conduct ablation studies targeting three core components: the design of hashing experts, expert sharing, and the role of the softmax mechanism. Table 6 summarizes the experimental results across three datasets.

Design of Hashing Experts vs. Traditional Experts.

Traditional Mixture of Experts (MoE) [28–31] typically employs two-layer MLPs with ReLU activations as experts, designed for general-purpose representation transformation. In contrast, our MoH replaces these with specialized hashing experts, which directly map the feature dimension to the hash bit dimension — effectively acting as task-specific hashing layers.

We compare two baselines: the traditional MoE expert, which uses a two-layer MLP with hidden ReLU as commonly seen in the MoE literature, and the traditional

Table 5. Performance of 1DNN+MoH and 2DNN+MoH on ImageNet, MSCOCO, and CIFAR-10 across all bits. Best results are **bolded**.

Method	ImageNet			MSCOCO			CIFAR-10		
	16 bits	32 bits	64 bits	16 bits	32 bits	64 bits	16 bits	32 bits	64 bits
2DNN+MoH	0.8601	0.8859	0.8996	0.7374	0.8217	0.8623	0.9632	0.9650	0.9647
1DNN+MoH	0.8744	0.8975	0.9062	0.7903	0.8675	0.8727	0.9665	0.9657	0.9658

hash expert, which consists of a single linear projection layer without non-linearity, as typically employed in hashing methods.

Our design strikes a balance: it retains the structure of two-layer MLPs but aligns their output directly to binary codes, offering greater representational power while preserving hash compatibility. As shown in the table, both traditional variants perform worse than our method, especially on MSCOCO (e.g., 0.8675 vs. 0.8472 for 32-bit).

Expert Sharing Across Branches. We adopt a shared expert design across branches in MoH to encourage consistent hashing and reduce redundancy. To verify its effectiveness, we compare with a variant where each branch has separate (unshared) experts.

Results show that unshared experts degrade performance on all datasets. For instance, on ImageNet at 32-bit, shared experts achieve 0.8975 vs. 0.8958 with unshared experts, confirming that expert sharing enhances generalization and code consistency.

Impact of Removing Softmax Gate. Unlike traditional MoE which utilizes softmax to weigh expert contributions, we remove softmax and instead allow parallel supervision from all experts. This simplifies optimization and encourages more diverse expert behaviors. As Table 6 shows, removing softmax leads to consistent improvements: for instance, on ImageNet (64-bit), performance rises from 0.9001 (with softmax) to 0.9062 (ours).

C.3. SM-MoH Parameter Tuning

We investigate the influence of two hyperparameters in the MoH module: the number of total experts (horizontal axis) and the activation ratio, i.e., the proportion of experts selected per input (vertical axis). As shown in Figure 7, each subfigure presents the model’s 16-bit mAP on CIFAR-10, ImageNet, and MSCOCO, respectively.

Overall, MoH demonstrates stable performance across a wide range of settings, but appropriate tuning of these parameters can yield noticeable improvements. On ImageNet, the best performance (0.8771 mAP) is achieved when using 64 experts with a 1/4 activation ratio, indicating a balanced trade-off between diversity and sparsity. On CIFAR-10, performance remains consistently high, with the best result (0.9666 mAP) also occurring at 64 experts and a 1/4 ratio. For MSCOCO, the highest mAP (0.7903) is observed

when activating 1/8 of 64 experts, suggesting that a smaller number of activated experts may be more effective.

It is also notable that overly low expert counts (e.g., 16) or excessively sparse activation (e.g., 1/8 on CIFAR-10) tend to hurt performance, likely due to insufficient model capacity or representational bottlenecks. These results suggest that MoH benefits from a moderate number of diverse experts, with partial activation to maintain efficiency and specialization.

D. Theory Supplement

Here we supplement discrepancy elimination theory in the main text: we derive an explicit inequality comparing the single-branch baseline risk R_{base} with the dual-branch Uni-Hash risk $R_{UniHash}$, provide a clean non-asymptotic sufficient condition under which $R_{UniHash} < R_{base}$, and show how these bounds ground our seen/unseen generalization analysis.

D.1. Risk Comparison: Baseline vs. UniHash

Risk decompositions. Let $R(\cdot)$ be population risk and $\hat{R}(\cdot)$ be empirical risk. For single-branch baselines and Uni-Hash, we have

$$R_{base} \leq \hat{R}_{base} + C_{stat}^{base} + C_{quant}^{base} + E_{struct}, \quad (18)$$

$$R_{UniHash} \leq \hat{R}_{UniHash} + C_{stat}^{UniHash} + C_{quant}^{UniHash} + C_{cons}. \quad (19)$$

Here, C_{stat} denotes capacity; C_{quant} is a quantization term decaying with code length; $E_{struct} > 0$ is the paradigm-specific structural error of single-branch training; and C_{cons} is the consistency term from mutual learning.

Capacity & consistency scalings. Under the assumptions already stated in the paper (Lipschitz modules and Top- k sparse routing), there exist constants such that

$$C_{stat}^{(\cdot)} = \mathcal{O}\left(\sqrt{\frac{k \log m}{n}}\right), \quad (20)$$

$$C_{quant}^{(\cdot)} = \exp(-\Omega(q)), \quad (21)$$

$$C_{cons} = \mathcal{O}\left(\frac{\tau}{\sqrt{n}}\right). \quad (22)$$

Table 6. Performance comparison of different methods on ImageNet, MSCOCO, and CIFAR-10 across all bits. Traditional MoE experts typically employ two-layer MLPs with ReLU activations. Traditional hashing expert consists of a single linear projection layer without non-linearity, as commonly used in hashing-based methods. Unshared expert indicates that the two branches do not share experts. "Trad" in this table means traditional. Best results are **bolded**.

Method	ImageNet			MSCOCO			CIFAR-10		
	16 bit	32 bit	64 bit	16 bit	32 bit	64 bit	16 bit	32 bit	64 bit
Trad MoE Expert	0.8762	0.8862	0.8942	0.7730	0.8472	0.8605	0.9649	0.9653	0.9634
Trad Hash Expert	0.8663	0.8872	0.8996	0.7584	0.8533	0.8658	0.9638	0.9641	0.9649
Unshared Expert	0.8728	0.8958	0.9031	0.7882	0.8657	0.8701	0.9658	0.9659	0.9657
With Softmax	0.8679	0.8907	0.9001	0.7793	0.8526	0.8686	0.9625	0.9639	0.9647
SM-MoH	0.8744	0.8975	0.9062	0.7903	0.8675	0.8727	0.9665	0.9657	0.9658

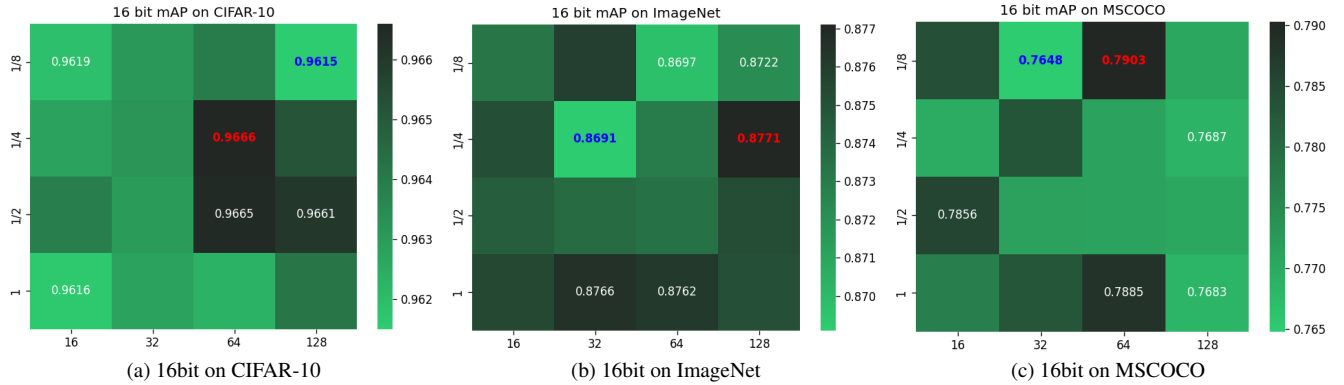


Figure 7. Impact of SM-MoH parameter tuning on model performance at 16-bit code length across ImageNet, MSCOCO, and CIFAR-10 datasets. In heatmaps, darker colors indicate higher values, while lighter colors represent lower values. The maximum and minimum values are highlighted in red and blue, respectively.

where n is sample size, m the number of experts, k the per-sample active experts, and $\tau^2 = \mathbb{E}\|u^c(x) - u^p(x)\|^2$ measures cross-branch mismatch.

Direct inequality for superiority. Subtracting Eq. 18 from Eq. 19 yields

$$R_{UniHash} - R_{base} \leq (\hat{R}_{UniHash} - \hat{R}_{base}) + (C_{stat}^{UniHash} - C_{stat}^{base}) + (C_{quant}^{UniHash} - C_{quant}^{base}) + (C_{cons} - E_{struct}). \quad (23)$$

Under the same backbone and bit settings, $C_{stat}^{UniHash} \approx C_{stat}^{base}$, $C_{quant}^{UniHash} \approx C_{quant}^{base}$, and with well-optimized training $\hat{R}_{UniHash} \approx \hat{R}_{base}$. Hence

$$R_{UniHash} - R_{base} \lesssim C_{cons} - E_{struct}. \quad (24)$$

Sufficient condition. If after training

$$C_{cons} < E_{struct} - \varepsilon \quad (\varepsilon > 0), \quad (25)$$

then Eq. 24 implies $R_{UniHash} < R_{base} - \varepsilon$. In effect, mutual learning replaces the irreducible single-branch structural error E_{struct} with a learnable consistency term C_{cons} . Once $C_{cons} < E_{struct}$, UniHash attains strictly lower population risk.

Asymptotics. When $n, q \rightarrow \infty$, Eq. 20–22 gives $C_{stat}, C_{cons} \rightarrow 0$ and $C_{quant} \rightarrow 0$, so from Eq. 19 we get $R_{UniHash} - \hat{R}_{UniHash} \rightarrow 0$; the single-branch bound Eq. 18 retains the constant floor $E_{struct} > 0$. Thus, by eliminating the structural floor that single-branch models retain, UniHash is strictly better asymptotically.

D.2. Seen/Unseen Generalization

Let $R_{seen}(\cdot)$ and $R_{unseen}(\cdot)$ be test risks on seen and unseen categories, and $\Delta(\cdot) = R_{unseen} - R_{seen}$ be the gap. View seen and unseen samples as drawn from $\mathcal{D}_s, \mathcal{D}_u$ on $(x, y) \in \mathcal{X} \times \mathcal{Y}$ with a shared \mathcal{X} but label sets \mathcal{Y}_s (seen) and \mathcal{Y}_u (unseen), where only \mathcal{Y}_s is observed in training; risks are expectations under \mathcal{D}_s or \mathcal{D}_u . For any hashing function f ,

$$R_{unseen}(f) \leq R_{seen}(f) + \text{disc}_{\mathcal{H}}(\mathcal{D}_s, \mathcal{D}_u) + \lambda(f). \quad (26)$$

where $\text{disc}_{\mathcal{H}}$ measures domain divergence w.r.t. hypothesis class \mathcal{H} , and $\lambda(f)$ captures how well the embedding's global anchors and relative layout transfer to unseen classes. Thus the gap $\Delta(f)$ is governed by (a) hypothesis complexity and (b) embedding alignment.

How UniHash reduces Δ . Mutual learning reduces the right-hand side of Eq. 26 along two coupled mechanisms. First, the cross-branch consistency term $C_{\text{cons}} = \mathcal{O}(\tau/\sqrt{n})$ enforces $u^c \approx u^p$, effectively contracting the admissible hypothesis class and thereby diminishing $\text{disc}_{\mathcal{H}}(\mathcal{D}_s, \mathcal{D}_u)$, since smaller classes are less sensitive to distribution shift. Second, training both branches in a single hash space with shared experts jointly supplies global anchors (pointwise signal) and relational geometry (pairwise signal), which improves semantic alignment on novel categories and lowers $\lambda(f)$; unseen samples are thus mapped onto the structured manifold spanned by seen semantics rather than drifting into uncalibrated regions.

Quantified gap reduction. Let f_{base} be a single-branch optimum and f_{UniHash} the UniHash solution. Combining Sec. D.1 with the two effects above yields

$$\Delta(f_{\text{UniHash}}) - \Delta(f_{\text{base}}) \lesssim C_{\text{cons}} - E_{\text{struct}} + \text{disc}_{\mathcal{H}_{\text{UniHash}}} - \text{disc}_{\mathcal{H}_{\text{base}}} + \lambda(f_{\text{UniHash}}) - \lambda(f_{\text{base}}). \quad (27)$$

If Eq. 25 holds and shared experts indeed align the embedding, the RHS is strictly negative: $\Delta(f_{\text{UniHash}}) < \Delta(f_{\text{base}})$. UniHash improves seen→unseen generalization by jointly shrinking the hypothesis-class sensitivity to distribution shift and enhancing semantic alignment. Concretely, the gap reduction in Eq. 27 follows from (i) consistency-driven capacity contraction, which lowers $\text{disc}_{\mathcal{H}}$, and (ii) shared-expert alignment, which reduces $\lambda(f)$. A simple non-asymptotic check (e.g., $C_{\text{cons}} < E_{\text{struct}}$ on validation) already guarantees a smaller unseen risk relative to single-branch baselines. As code length increases, quantization errors decay and further facilitate these effects, and asymptotically UniHash removes the structural floor retained by single-branch training, yielding strictly better population risk on unseen classes.

E. Limitations

While our proposed Unified Hashing (UniHash) consistently demonstrates strong performance across diverse datasets and settings, several complementary aspects remain open for further exploration. First, the dual-branch architecture and the SM-MoH module introduce a more intricate interaction mechanism in the hash code generation process, which makes the interpretability of individual bits less straightforward. Second, like many deep hashing methods, UniHash may encounter practical limitations in resource-constrained environments due to its reliance on deep neural networks. However, as numerous methods exist to improve the deployability of deep neural networks, this limitation has been less significant. These considerations highlight valuable directions for future work while underscoring the effectiveness of our method.

References

- [1] P. Li, A. Shrivastava, J. Moore, and A. König. Hashing algorithms for large-scale learning. *Advances in Neural Information Processing Systems (NeurIPS)*, 24, 2011. 1
- [2] Z. Jiang, Z. Weng, R. Li, H. Zhuang, and Z. Lin. Online weighted hashing for cross-modal retrieval. *Pattern Recognition*, 161:111232, 2025.
- [3] Y. Cao, X. Chen, Z. Liu, W. Jia, F. Meng, and J. Gui. Deep graph online hashing for multi-label image retrieval. In *Proceedings of the AAAI Conference on Artificial Intelligence (AAAI)*, volume 39, pages 1953–1961, 2025.
- [4] M. Liang, J. Du, Z. Liang, Y. Xing, W. Huang, and Z. Xue. Self-supervised multi-modal knowledge graph contrastive hashing for cross-modal search. In *Proceedings of the AAAI Conference on Artificial Intelligence (AAAI)*, volume 38, pages 13744–13753, 2024.
- [5] F. Kong, S. Yuan, W. Hao, and R. Henao. Mitigating test-time bias for fair image retrieval. *Advances in Neural Information Processing Systems (NeurIPS)*, 36, 2024.
- [6] P. Wu, S. Wang, K. D. Rosa, and D. Hu. Forb: A flat object retrieval benchmark for universal image embedding. *Advances in Neural Information Processing Systems (NeurIPS)*, 36:25448–25460, 2023. 1
- [7] Y. Cao, M. Long, B. Liu, and J. Wang. Deep cauchy hashing for hamming space retrieval. In *Proceedings of the IEEE Conference on Computer Vision and Pattern Recognition (CVPR)*, pages 1229–1237, 2018. 1
- [8] E. Yang, T. Liu, C. Deng, and D. Tao. Adversarial examples for hamming space search. *IEEE Transactions on Cybernetics*, 50(4):1473–1484, 2018.
- [9] J. Qin, Y. Wang, C. Xiao, W. Wang, X. Lin, and Y. Ishikawa. Gph: Similarity search in hamming space. In *Proceedings of the IEEE International Conference on Data Engineering (ICDE)*, pages 29–40, 2018.
- [10] H. Jégou, M. Douze, and C. Schmid. Hamming embedding and weak geometric consistency for large scale image search. In *Proceedings of the European Conference on Computer Vision (ECCV)*, pages 304–317, 2008. 1
- [11] L. Yuan, T. Wang, X. Zhang, F. E. H. Tay, Z. Jie, W. Liu, and J. Feng. Central similarity quantization for efficient image and video retrieval. In *Proceedings of the IEEE/CVF Conference on Computer Vision and Pattern Recognition (CVPR)*, pages 3083–3092, 2020. 1, 2, 5, 6, 7
- [12] J. T. Hoe, K. W. Ng, T. Zhang, C. S. Chan, Y.-Z. Song, and T. Xiang. One loss for all: Deep hashing

with a single cosine similarity based learning objective. *Advances in Neural Information Processing Systems (NeurIPS)*, 34:24286–24298, 2021. [2](#), [6](#), [7](#)

[13] L. Wang, Y. Pan, C. Liu, H. Lai, J. Yin, and Y. Liu. Deep hashing with minimal-distance-separated hash centers. In *Proceedings of the IEEE/CVF Conference on Computer Vision and Pattern Recognition (CVPR)*, pages 23455–23464, 2023. [1](#), [2](#), [5](#), [6](#), [7](#), [8](#)

[14] L. He, Y. Zhang, R. Li, Z. Huang, R. Wu, and E. Chen. A flexible plug-and-play module for generating variable-length. *arXiv preprint arXiv:2412.08922*, 2024.

[15] H. Liu, R. Wang, S. Shan, and X. Chen. Deep supervised hashing for fast image retrieval. In *Proceedings of the IEEE Conference on Computer Vision and Pattern Recognition (CVPR)*, pages 2064–2072, 2016. [1](#), [5](#), [6](#), [7](#)

[16] W.-J. Li, S. Wang, and W.-C. Kang. Feature learning based deep supervised hashing with pairwise labels. In *Proceedings of the Twenty-Fifth International Joint Conference on Artificial Intelligence (IJCAI)*, pages 1711–1717, 2016. [6](#), [7](#)

[17] Z. Cao, M. Long, J. Wang, and P. S. Yu. Hashnet: Deep learning to hash by continuation. In *Proceedings of the IEEE International Conference on Computer Vision (ICCV)*, pages 5608–5617, 2017. [1](#), [2](#), [6](#), [7](#)

[18] X. Wang, Y. Shi, and K. M. Kitani. Deep supervised hashing with triplet labels. In *Proceedings of the Asian Conference on Computer Vision (ACCV)*, pages 70–84, 2017. [1](#), [6](#), [7](#)

[19] S. Su, C. Zhang, K. Han, and Y. Tian. Greedy hash: Towards fast optimization for accurate hash coding in cnn. *Advances in Neural Information Processing Systems (NeurIPS)*, 31, 2018. [6](#), [7](#)

[20] L. Fan, K. W. Ng, C. Ju, T. Zhang, and C. S. Chan. Deep polarized network for supervised learning of accurate binary hashing codes. In *Proceedings of the International Joint Conference on Artificial Intelligence (IJCAI)*, pages 825–831, 2020. [1](#), [5](#), [6](#), [7](#)

[21] J. Wei, S. Wang, S. K. Zhou, S. Cui, and Z. Li. Weakly supervised object localization through inter-class feature similarity and intra-class appearance consistency. In *Proceedings of the European Conference on Computer Vision (ECCV)*, pages 195–210, 2022. [1](#)

[22] S. Xuan and S. Zhang. Intra-inter camera similarity for unsupervised person re-identification. In *Proceedings of the IEEE/CVF Conference on Computer Vision and Pattern Recognition (CVPR)*, pages 11926–11935, 2021.

[23] T. Kobayashi. T-vmf similarity for regularizing intra-class feature distribution. In *Proceedings of the IEEE/CVF Conference on Computer Vision and Pattern Recognition (CVPR)*, pages 6616–6625, 2021. [1](#)

[24] J. Wang and X.-L. Zhang. Improving pseudo labels with intra-class similarity for unsupervised domain adaptation. *Pattern Recognition*, 138:109379, 2023. doi: 10.1016/j.patcog.2023.109379. [1](#)

[25] Y. Shen, P. Wang, X.-S. Wei, and Y. Yao. An empirical study on training paradigms for deep supervised hashing. *International Journal of Computer Vision (IJCV)*, pages 1–39, 2025. [1](#), [2](#), [6](#), [10](#)

[26] C. Deng, Z. Chen, X. Liu, X. Gao, and D. Tao. Triplet-based deep hashing network for cross-modal retrieval. *IEEE Transactions on Image Processing*, 27(8):3893–3903, 2018. doi: 10.1109/TIP.2018.2821921. [1](#)

[27] Y. Liang, Y. Pan, H. Lai, W. Liu, and J. Yin. Deep list-wise triplet hashing for fine-grained image retrieval. *IEEE Transactions on Image Processing*, 31:949–961, 2021. [1](#)

[28] N. Shazeer, A. Mirhoseini, K. Maziarz, A. Davis, Q. Le, G. Hinton, and J. Dean. Outrageously large neural networks: The sparsely-gated mixture-of-experts layer. *arXiv preprint arXiv:1701.06538*, 2017. [2](#), [10](#)

[29] T. Chen, X. Chen, X. Du, A. Rashwan, F. Yang, H. Chen, Z. Wang, and Y. Li. Adamv-moe: Adaptive multi-task vision mixture-of-experts. In *Proceedings of the IEEE/CVF International Conference on Computer Vision (ICCV)*, pages 17346–17357, 2023. [2](#)

[30] Z. Chen, Y. Deng, Y. Wu, Q. Gu, and Y. Li. Towards understanding the mixture-of-experts layer in deep learning. *Advances in Neural Information Processing Systems (NeurIPS)*, 35:23049–23062, 2022.

[31] C. Riquelme, J. Puigcerver, B. Mustafa, M. Neumann, R. Jenatton, A. S. Pinto, D. Keysers, and N. Houlsby. Scaling vision with sparse mixture of experts. *Advances in Neural Information Processing Systems (NeurIPS)*, 34:8583–8595, 2021. [2](#), [10](#)

[32] V. E. Lio, J. Lu, G. Wang, P. Moulin, and J. Zhou. Deep hashing for compact binary codes learning. In *Proceedings of the IEEE Conference on Computer Vision and Pattern Recognition (CVPR)*, pages 2475–2483, 2015. [2](#)

[33] Y. Zhang, T. Xiang, T. M. Hospedales, and H. Lu. Deep mutual learning. In *Proceedings of the IEEE Conference on Computer Vision and Pattern Recognition (CVPR)*, pages 4320–4328, 2018. [2](#), [10](#)

[34] H. Zhao, G. Yang, D. Wang, and H. Lu. Deep mutual learning for visual object tracking. *Pattern Recognition*, 112:107796, 2021. [2](#), [10](#)

[35] Y. Guo, B. Liu, and D. Zhao. Online continual learning through mutual information maximization. In *Proceedings of the International Conference on Machine Learning (ICML)*, pages 8109–8126, 2022.

- [36] B. Zhao and K. Han. Novel visual category discovery with dual ranking statistics and mutual knowledge distillation. *Advances in Neural Information Processing Systems (NeurIPS)*, 34:22982–22994, 2021. [2](#), [10](#)
- [37] A. Krizhevsky and G. Hinton. Learning multiple layers of features from tiny images. *Technical Report, University of Toronto*, 2009. [5](#), [10](#)
- [38] J. Deng, W. Dong, R. Socher, L.-J. Li, K. Li, and L. Fei-Fei. Imagenet: A large-scale hierarchical image database. In *Proceedings of the IEEE Conference on Computer Vision and Pattern Recognition (CVPR)*, pages 248–255, 2009. [5](#), [10](#)
- [39] T.-Y. Lin, M. Maire, S. Belongie, J. Hays, P. Perona, D. Ramanan, P. Dollár, and C. L. Zitnick. Microsoft coco: Common objects in context. In *Proceedings of the European Conference on Computer Vision (ECCV)*, pages 740–755, 2014. [5](#), [10](#)
- [40] K. He, X. Zhang, S. Ren, and J. Sun. Deep residual learning for image recognition. In *Proceedings of the IEEE Conference on Computer Vision and Pattern Recognition (CVPR)*, pages 770–778, 2016. [6](#)
- [41] A. F. Agarap. Deep learning using rectified linear units (relu). *arXiv preprint arXiv:1803.08375*, 2019. [6](#)
- [42] X. Xiang, X. Ding, L. Jin, Z. Li, J. Tang, and R. Jain. Alleviating over-fitting in hashing-based fine-grained image retrieval: From causal feature learning to binary-injected hash learning. *IEEE Transactions on Multimedia*, 26:10665–10677, 2024. [7](#)
- [43] Yue Cao, Mingsheng Long, and Jianmin Wang. Correlation hashing network for efficient cross-modal retrieval. In *British Machine Vision Conference, BMVC*, 2017. [7](#)
- [44] Xiu-Shen Wei, Yang Shen, Xuhao Sun, Peng Wang, and Yuxin Peng. Attribute-aware deep hashing with self-consistency for large-scale fine-grained image retrieval. *IEEE Transactions on Pattern Analysis and Machine Intelligence*, 45(11):13904–13920, 2023. [6](#)
- [45] Laurens van der Maaten and Geoffrey Hinton. Visualizing data using t-SNE. *Journal of Machine Learning Research*, 9(86):2579–2605, 2008. [8](#)
- [46] X. Zheng, Y. Zhang, and X. Lu. Deep balanced discrete hashing for image retrieval. *Neurocomputing*, 403:224–236, 2020. [8](#)
- [47] R. Wu, M. Feng, W. Guan, D. Wang, H. Lu, and E. Ding. A mutual learning method for salient object detection with intertwined multi-supervision. In *Proceedings of the IEEE/CVF Conference on Computer Vision and Pattern Recognition (CVPR)*, pages 8150–8159, 2019. [10](#)